Research Square

Preprints are preliminary reports that have not undergone peer review.
They should not be considered conclusive, used to inform clinical practice,
or referenced by the media as validated information.

Microstructure-Induced Variability in Residence Time Distributions of Fibrous Porous Media

E.G. Karvelas

ekarvelas@uniwa.gr

University of West Attica

A. Tsiantis

University of Thessaly

P. Chatzisaroglou

University of Thessaly

T.D. Papathanasiou

University of Thessaly

Research Article

Keywords: Residence Time Distribution, Computational fluid dynamics, Effective Peclet number, Biomedical transport modeling, Microstructure-induced dispersion

Posted Date: September 7th, 2026

DOI: https://doi.org/10.21203/rs.3.rs-10827788/v1

License: This work is licensed under a Creative Commons Attribution 4.0 International License.
Read Full License

Additional Declarations: No competing interests reported.

Article Highlights

- Fiber spatial arrangement, not density alone, controls how predictably fluid moves through fibrous porous media.
- Clustered fiber microstructures cause long transit-time tails and reduced transport predictability.
- Ordered fiber lattices show the most uniform, near plug-flow transport of the three arrangements tested.

Microstructure-Induced Variability in Residence Time Distributions of Fibrous Porous Media

E.G. Karvelas[1*], A. Tsiantis[2], P. Chatzisaroglou[2], T.D. Papathanasiou[2]

[1*]Department of Biomedical Engineering, University of West Attica, 12243, Athens, Greece.
[2]Department of Mechanical Engineering, University of Thessaly, Pedion Areos, 38221, Volos, Greece.

*Corresponding author(s). E-mail(s): ekarvelas@uniwa.gr;

Abstract

Biological tissues consist of cells embedded within a fibrous extracellular matrix (***ECM***) that governs both mechanical support and solute transport. This study examines how fiber arrangement, volume fraction, and Peclet number affect hydraulic permeability and residence time statistics in idealized fibrous geometries, using computational fluid dynamics (***CFD***) in OpenFOAM to solve convection-diffusion transport for a passive tracer. Steady velocity fields were obtained for hexagonal, random, and clustered fiber configurations, followed by transient solution of the tracer transport equation and moment-based analysis of the resulting residence time distributions (***RTDs***). Ordered hexagonal arrangements produce narrowly distributed ***RTDs*** with effective Peclet numbers up to an order of magnitude higher than random arrangements at identical nominal Peclet number and volume fraction, indicating near plug-flow behavior. Clustered microstructures generate pronounced right-skewed ***RTDs***, elevated mean residence times, and a marked reduction in effective Peclet number, reflecting increased dispersion from spatially correlated low-velocity regions. This finding shows that microstructural organization, not volume fraction alone, is a primary determinant of transport variability in fibrous porous media. This is relevant to the design of fibrous materials generally, including engineered scaffolds and drug-delivery carriers, where transport predictability matters.

Keywords: Residence Time Distribution, Computational fluid dynamics, Effective Peclet number, Biomedical transport modeling, Microstructure-induced dispersion

1 Introduction

Biological tissues are hierarchical structures in which cells are embedded in an ECM that provides mechanical support and mediates the transport of nutrients, oxygen, and signaling molecules. The $ECM's$ composition – collagen, elastin, glycosaminoglycans, and proteoglycans – underlies its structural role and its function in cell-ECM communication and tissue homeostasis Hu et al. (2022); Huang et al. (2021).

This transport occurs under coupled diffusion and convection at the low Reynolds numbers ($Re \ll 1$) typical of biological environments Bear (1972); Dullien (2012), where viscous forces dominate and convective solute transport is superimposed on a predictable laminar flow. Characterizing solute transport under these coupled conditions offers insight into the processes governing cellular environments and tissue function Kamm (1999); Jain (1987).

Due to their fibrous nature, biological tissues can be effectively modeled as fiber media, allowing porous-media and fiber-flow theory to be applied in a biological context Sahimi (2011). The porosity, tortuosity, and permeability of the inter-fiber pathways are critical, tissue and pathology dependent determinants of nutrient, oxygen, and waste transport efficiency Dutta and Tarbell (1996); Carmeliet and Jain (2000), with fiber orientation and density strongly influencing tissue health and function Murray (1926); Jain (2005). This diffusion-driven transport directly informs tissue engineering scaffold design and diffusion-based drug delivery Griffith and Swartz (2006); Saltzman (2001); Langer (1998).

A recent study on the effect of micropolar fluid properties on the hydraulic permeability of fibrous biomaterials Karvelas et al. (2020) highlighted the impact of fiber arrangement and density on diffusion, while a computational study on collagen fibril diameter distribution underscored the role of microstructural variation between healthy and injured tissue in determining permeability Erisken et al. (2020). However, these studies characterized steady permeability only, leaving unexamined how the same microstructural variables shape the transient, statistical spread of solute transit times.

The RTD curve is a cornerstone for analyzing mixing in fixed-bed reactors and porous contactors Bhaskar and Singh (2018), quantifying the relative contributions of convection and diffusion via the Peclet number (Pe). Traditional RTD models assume uniform (plug) flow and a spatially uniform diffusion coefficient (D), while real fibrous media violate the first assumption, as irregular fiber arrangement creates preferential flow channels, or "rivers" Markicevic and Papathanasiou (2003, 2004). The present study retains the uniform D assumption, although apparent diffusivity is known to vary with local packing density in real tissue Burada et al. (2009); Hamada et al. (2020). This isolates the transport variability reported here to microstructural arrangement and volume fraction alone.

This study investigates diffusion-driven transport at low Reynolds numbers in biological tissues modeled as fiber media, examining how fibril arrangement, volume fraction, and Peclet number affect hydraulic permeability and species transport dynamics. Beyond qualitative breakthrough-curve analysis, a moment-based RTD framework quantifies mean transit times, transport variance, and effective Peclet

numbers. Section 2 presents the numerical methodology and geometry generation procedure, while Section 3 reports the effects of fiber arrangement, volume fraction, and Peclet number on the RTD. Section 4 discusses the findings and limitations, and Section 5 presents the conclusions.

2 Materials and Methods

2.1 Unit cell definition

In this study, geometries consisting of a unit cell were simulated with a size of $L \times H$ where L and H represent the length and the height of the cell, respectively. Fibers were placed inside the unit cell in hexagonal, random, and clustered distributions. Hexagonal coordinates were fixed at equal inter-fiber distances while random distributions were generated by a Random Sequential Addition (RSA) procedure Tsiantis and Papathanasiou (2019). Finally, clustered distributions were generated by molecular dynamics simulation. Fiber size was fixed at 10 μm and unit cell length at 1 mm. The fiber volume fraction (ϕ) is defined as:

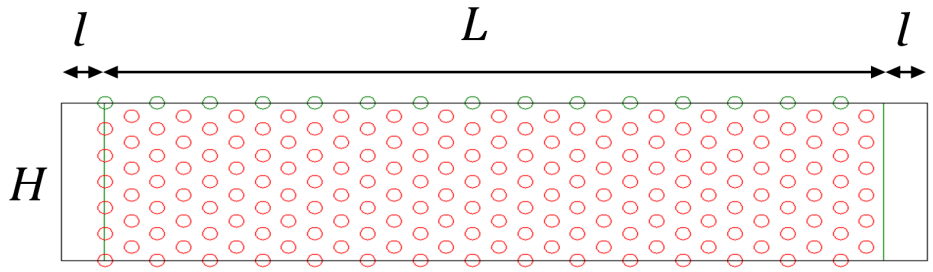
$$\phi = \frac{N\pi r^2}{LH} \tag{1}$$

where N is the number of fibers inside the unit cell, r is the fiber radius and L, H are the effective dimensions of the unit cell. A small edge region of length l was added along the X direction of each unit cell to avoid boundary artifacts from fibers placed too close to the edge and to prevent degenerate mesh elements. This addition had a negligible effect on the results and was excluded when computing ϕ and N. Species transport is implicitly assumed to occur perpendicular to the fiber axis. A hexagonal and a random geometry are shown in Fig. 1.

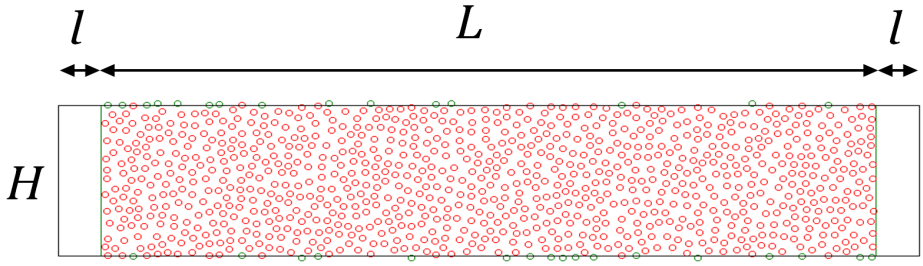
All unit cells used an aspect ratio of $L/H = 5$, which was found to balance computational cost against the accuracy afforded by periodic boundary conditions Hassani and Hinton (1998, 1999). Larger aspect ratios failed to yield uniform random fiber distributions, while smaller ratios gave no significant accuracy gain but increased computational cost. Since fiber radius was fixed within each simulation, the number of fibers N was set via Eq. 1 to achieve the desired ϕ, with a sufficient fiber count maintained throughout to avoid non-uniform distributions and associated statistical artifacts.

2.2 Geometry generation

Simulation geometries and case files were generated with an in-house application. First, the required number of fibers was determined from Eq. 1. Fibers were then positioned using the RSA algorithm, which randomly places discs (with periodic mirror images near the boundary) and accepts each placement only if it does not overlap previously placed fibers, until the target count is reached. The RSA jamming limit for disks, $\phi \approx 0.547$ Feder (1980); Hinrichsen et al. (1986), is well above the volume fractions used here, so no special measures were needed to reach the desired ϕ. In addition, a safety distance of 5% of the disc radius between fibers was enforced to avoid degenerate mesh elements. Resulting geometries were meshed with GMSH Geuzaine and Remacle



a)



b)

Fig. 1: Geometries used in simulations with hexagonal and random arrangement of fibers. The geometry of the unit cell is periodic and the fibers that are added for the construction of the periodic geometry are shown in the upper side of the unit cells with green color. The area of length l that was added for the avoidance of edge effects is also presented a) Hexagonal geometry with $\phi = 0.2, L = 1, H = 0.2$ and $N = 238$. b) Random geometry with $\phi = 0.2, L = 1, H = 0.2$ and $N = 907$.

(2009). For hexagonal geometries, fiber positions were instead fixed a priori from the geometrical relations:

$$h = 2R, v = R \tag{2}$$

where R is the fiber radius and h, v are the horizontal and vertical inter-fiber spacings.

Clustered arrangements were generated via molecular dynamics in $HOOMD-blue$ Anderson et al. (2020), using NVT/Langevin dynamics to aggregate fibers under a reduced temperature T^*. Low T^* drives strong aggregation, higher T^* yields near-random distributions. The degree of clustering at each T^* was quantified against the Poisson (complete spatial randomness) benchmark via a microstructure distribution (MD) index, and geometries with excessive aggregation (a single dominant cluster or cluster size comparable to the unit cell) were excluded as unrepresentative.

2.3 Numerical model

All simulations were performed using OpenFOAM Weller et al. (1998). The steady incompressible flow field was obtained by solving the continuity and Navier-Stokes equations:

$$\nabla \cdot \vec{u} = 0 \tag{3}$$

$$\vec{u} \cdot \nabla \vec{u} = -\frac{1}{\rho} \nabla p + \nu \nabla^2 \vec{u} \tag{4}$$

where $\vec{u}$ is the flow velocity vector, ρ is the fluid density, p is the pressure and ν is the kinematic viscosity, using the $SIMPLE$ algorithm for pressure-velocity coupling with water as the working fluid. A constant non-dimensional pressure drop of 1 was imposed across each geometry (inlet $p = 1$, outlet $p = 0$, zero-gradient velocity at both), with periodic conditions on the remaining boundaries and no-slip for $\vec{u}$ and zero-gradient for p at fiber surfaces. Iterations were performed until pressure and velocity residuals fell by nine orders of magnitude. An unstructured quad-dominant hybrid mesh of approximately 4×10^6 cells, locally refined around fibers (Fig. 2), was used. A mesh independence study was performed via Richardson extrapolation over 0.5–4×10^6 cells (Table 1), giving a discretization error of 1.25% in permeability at the working mesh density relative to the extrapolated infinite-mesh estimate. As permeability deviation is scale-invariant with respect to fluid viscosity under Darcy's law, this discretization error is representative of the water-based simulations reported throughout this study.

Table 1: Mesh independence study: deviation in hydraulic permeability as a function of mesh resolution, assessed via Richardson extrapolation relative to the infinite-mesh estimate (Grid 0).

Grid	Total cells	Deviation from Richardson estimate
0 (Richardson-extrapolated)	∞	–
1 (working mesh)	$\sim 4 \times 10^6$	1.25%
2	$\sim 2 \times 10^6$	2.40%
3	$\sim 1 \times 10^6$	4.58%
4	$\sim 0.5 \times 10^6$	7.61%

The flow domain is two-dimensional. Since the governing equations involve only in-plane velocity and a scalar pressure field, with no out-of-plane microrotation coupling as in micropolar flow Karvelas et al. (2020), the resulting field for these transversally-uniform fiber geometries is exactly representable by a $2D$ cross-section, consistent with standard practice for transverse permeability studies of unidirectional fiber arrays Papathanasiou (1996); Papathanasiou and Lee (1997).

Tracer transport was modeled on the converged steady velocity field by solving the unsteady convection-diffusion equation with an Euler implicit time scheme:

$$\frac{\partial C}{\partial t} + \nabla \cdot (UC) - \nabla^2 (D_C C) = 0 \tag{5}$$

where C is the species concentration, U the local fluid velocity, and D_C the molecular diffusion coefficient. Periodic conditions were imposed at the front, back, top and bottom boundaries. A fixed concentration of $C = 1$ was set at the inlet, with zero-gradient conditions at the outlet and at fiber surfaces. The Pe is defined as:

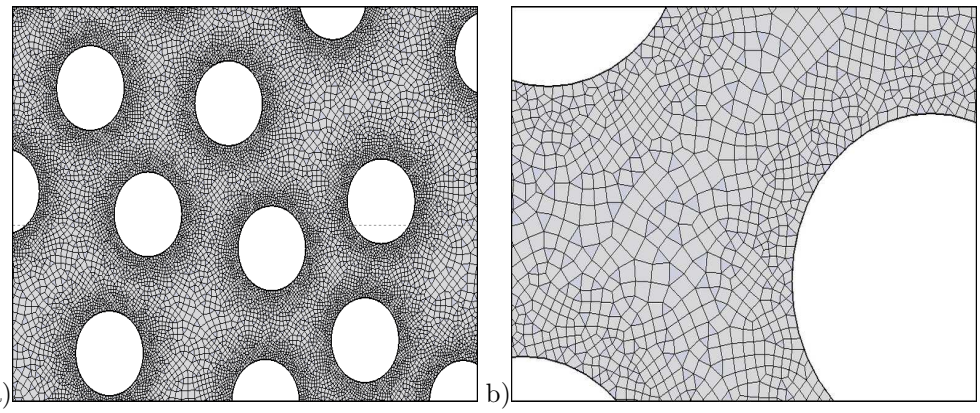


Fig. 2: a) Focused view of the computational mesh and b) Magnification of the computational mesh among the fibers.

$$Pe = \frac{UL}{D_C} \tag{6}$$

U is the mean interstitial velocity and L the unit cell length. The tracer concentration at the outlet was recorded over time as the step-response (breakthrough) curve $C(t)$. The residence time distribution is $E(t) = dC/dt$, normalized as $E(\theta)$ with $\theta = t^*/\langle t^* \rangle$ and $t^* = t \cdot U/[(1-\phi)L]$. The effective Peclet number was computed as $Pe_{eff} = 2/\sigma_\theta^2$, where σ_θ^2 is the variance of the normalized RTD. These quantities – $E(\theta)$, $\langle t^* \rangle$, and Pe_{eff} – constitute the moment-based RTD framework applied throughout Sections 3.1 and 4.

2.4 Model validation

The flow solver was previously validated against Gebart's analytical model for the transverse permeability of periodic fiber arrays, based on the lubrication approximation Gebart (1992), agreeing to within 10% at low volume fractions ($\phi = 0.1, 0.2$) with diminishing discrepancy as ϕ increased Karvelas et al. (2020). This validates the flow-field methodology common to the present study. The passive-scalar transport algorithm implements the standard finite-volume discretization of Eq. 5 using established OpenFOAM numerical schemes.

3 Results

In this study, biological tissues were modeled as fibrous media to examine their transport phenomena. These were investigated through a series of simulations, focusing on how fiber arrangement, ϕ, and Pe govern hydraulic permeability and $RTDs$. Breakthrough curves give a first, qualitative indication of transport character, with sharper curves reflecting convection-dominated transport and broader curves reflecting diffusion-dominated transport. For a quantitative, scale-consistent comparison across microstructures, the moment-based RTD framework is then applied.

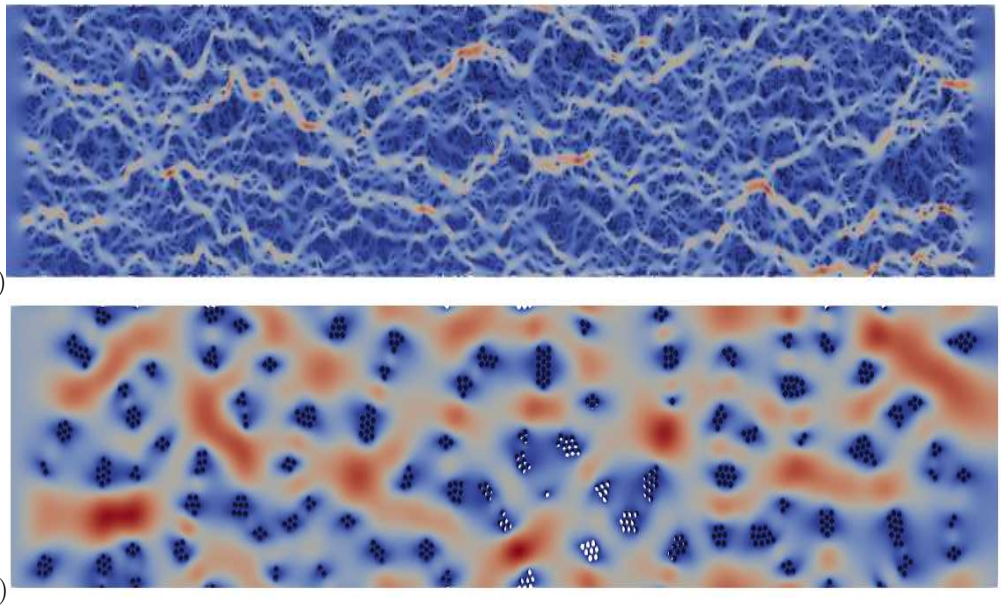


Fig. 3: Velocity of the fluid in geometry with a) random arrangement and b) cluster arrangement of fibers.

The velocity field for random and clustered fiber arrangements is shown in Fig. 3. The random arrangement produces a non-uniform velocity field with preferential flow channels or "rivers," arising from irregular inter-fiber spacing (Fig. 3a). The clustered arrangement shows more pronounced heterogeneity, with dense fiber regions creating extended stagnation zones alongside faster free-flow pathways (Fig. 3b), indicating that fluid transport is strongly governed by microstructural arrangement rather than fiber density alone.

Tracer concentration profiles at the exit of hexagonal geometries are shown as a function of time (Fig. 4) and of dimensionless time t^* (Fig. 5) for a range of Pe across volume fractions $\phi = 0.1$–0.35. At low Pe (0.01), diffusion dominates and the breakthrough curves are broad, with volume fraction only mildly shifting the mean breakthrough time (Fig. 4a, 5a). As Pe increases, the curves progressively sharpen, reflecting the growing role of convection, while the sensitivity to ϕ diminishes. When $Pe = 5$, the curves are narrow and nearly ϕ-independent (Fig. 4d, 5d), consistent with the transition to convection-dominated, near plug-flow transport. Across all Pe, higher ϕ consistently delays breakthrough, though the effect is most pronounced at low Pe.

In strongly convection-dominated regimes ($Pe = 5$), the ordered hexagonal configuration approaches quasi plug-flow behavior with minimal sensitivity to geometric heterogeneity. The random and clustered configurations were therefore examined at $Pe = 1$, where advective and diffusive mechanisms are comparable and microstructural organization exerts a measurable influence on transit-time variability.

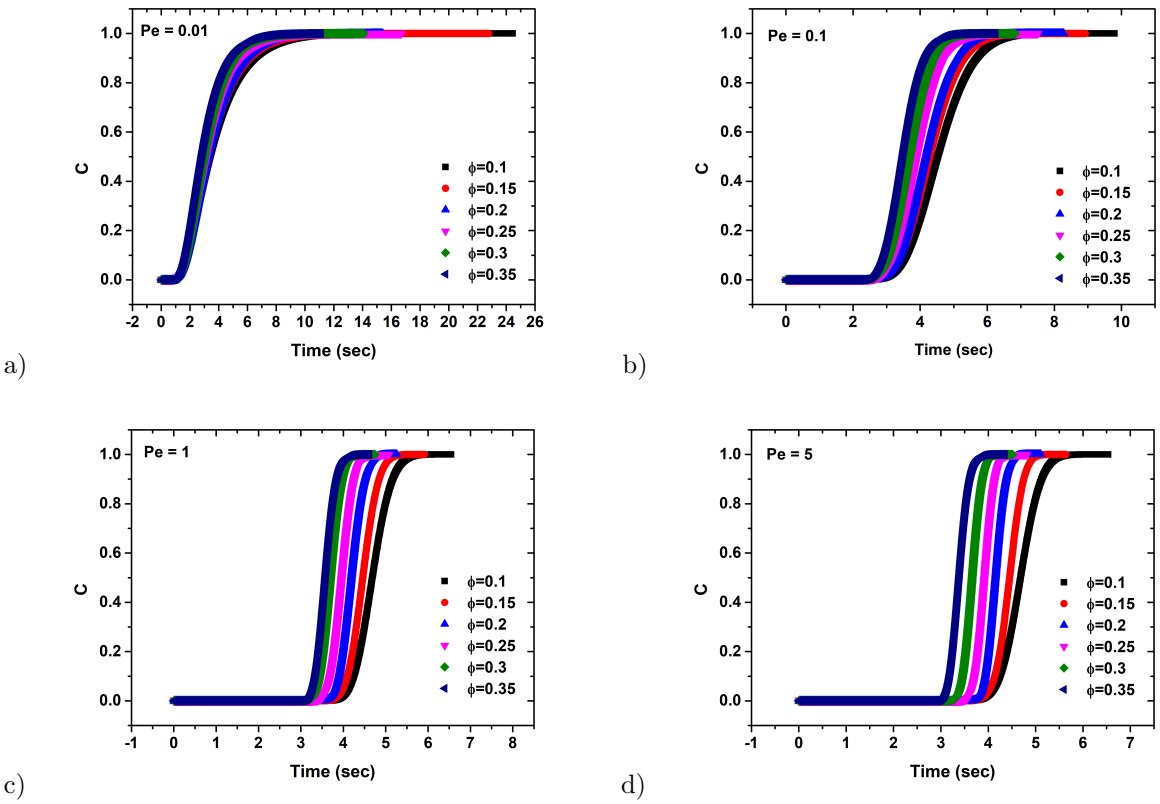


Fig. 4: Residence time (t) of the evolution of tracer concentration C in hexagonal arrangement of fibers under different volume fractions for a)$Pe = 0.01$, b) $Pe = 0.1$, c) $Pe = 1$, d) $Pe = 5$.

For the random arrangement (Fig. 6), increasing ϕ delays both the breakthrough time and its dimensionless counterpart, with the curves showing a slightly irregular, broadened shape that reflects transport variability introduced by the disordered geometry.

For the clustered arrangement (Fig. 7), increasing ϕ produces a much stronger delay in breakthrough time than in the hexagonal or random cases, together with pronounced curve irregularity – indicating that, unlike in ordered or random arrays, transport in clustered media is strongly ϕ-dependent.

3.1 Transit-Time Variability and Microstructural Effects

For the ordered (hexagonal) arrangement, RTDs remain narrow and sharply peaked around $\theta \approx 1$, indicating near plug-flow behavior (Fig. 8a). As ϕ increases from 0.1 to 0.3, only a slight rightward shift and mild broadening occur, with $\langle t^* \rangle$ rising gradually

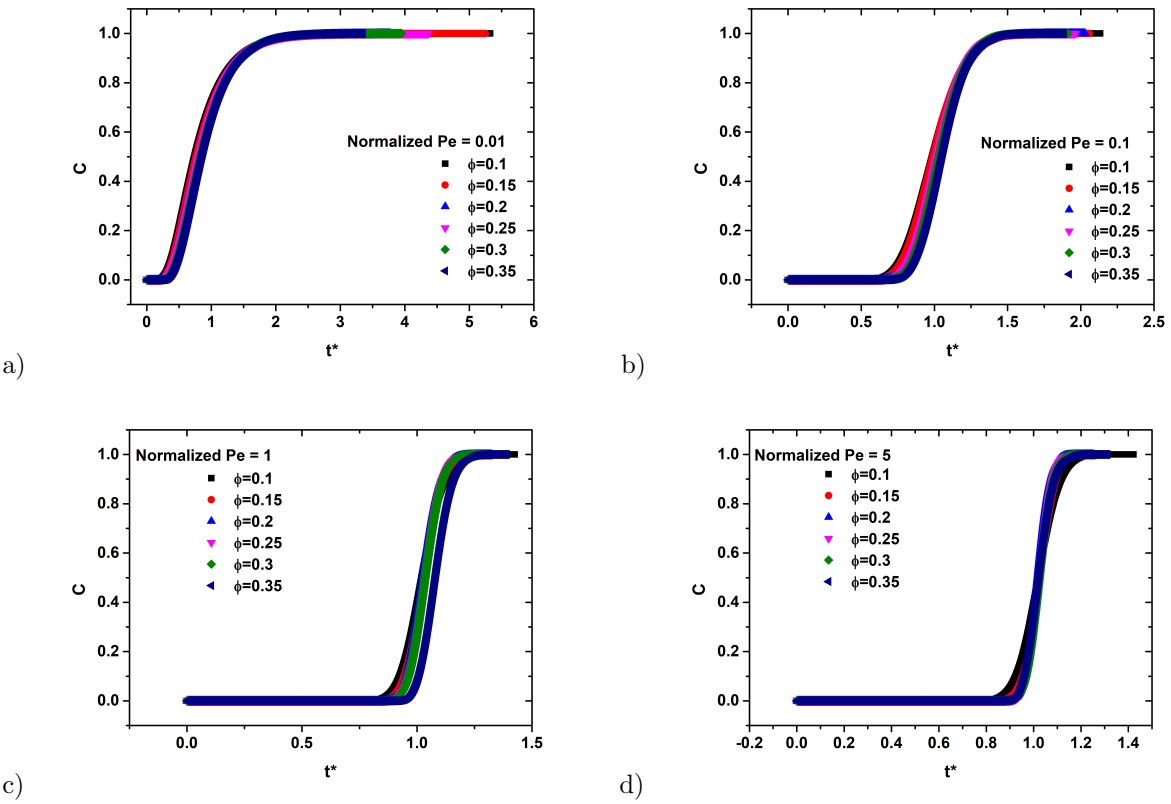


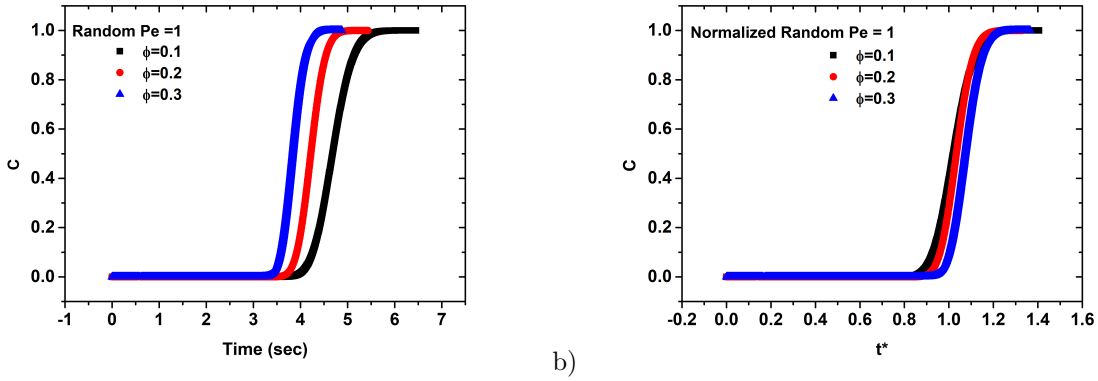
Fig. 5: Concentration profiles at the exit of the unit cell as function of the dimensionless time (t^*) for various values of (ϕ) in hexagonal arrangement of fibers for a) $Pe = 0.01$, b) $Pe = 0.1$, c) $Pe = 1$, d) $Pe = 5$.

(Fig. 9) and Pe_{eff} decreasing moderately (Fig. 10), reflecting a modest increase in dispersion while advective coherence is largely preserved.

The random microstructure produces broader RTDs than the ordered case, with the peak flattening and shifting to higher θ as ϕ increases (Fig. 8a). The corresponding rise in $\langle t^* \rangle$ is more pronounced than for the hexagonal case (Fig. 9a), and Pe_{eff} falls accordingly (Fig. 10a), reflecting greater sensitivity to velocity-field heterogeneity from random fiber placement.

The clustered arrangement is qualitatively different. RTDs become strongly right-skewed with tails that grow markedly with ϕ (Fig. 8b), reflecting the emergence of slow pathways and localized retention zones. The normalized RTD broadens sharply with ϕ (Fig. 9b) while Pe_{eff} drops steeply (Fig. 10b), indicating substantial loss of advective coherence and strongly enhanced dispersion.

All these results reveal a hierarchical influence of microstructural organization on transport variability. The ordered structures produce coherent, narrowly distributed



a) b)

Fig. 6: a) Residence (t) and b) dimensionless (t^*) time of tracer concentration C for random arrangement of fibers.

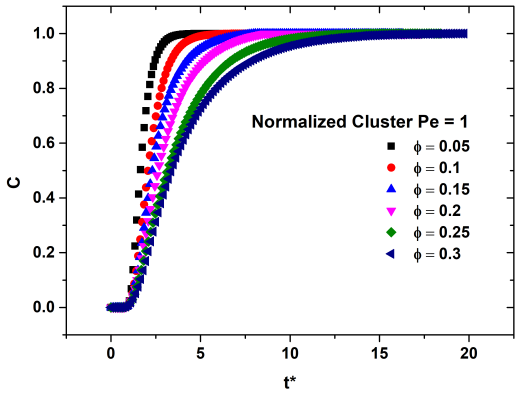
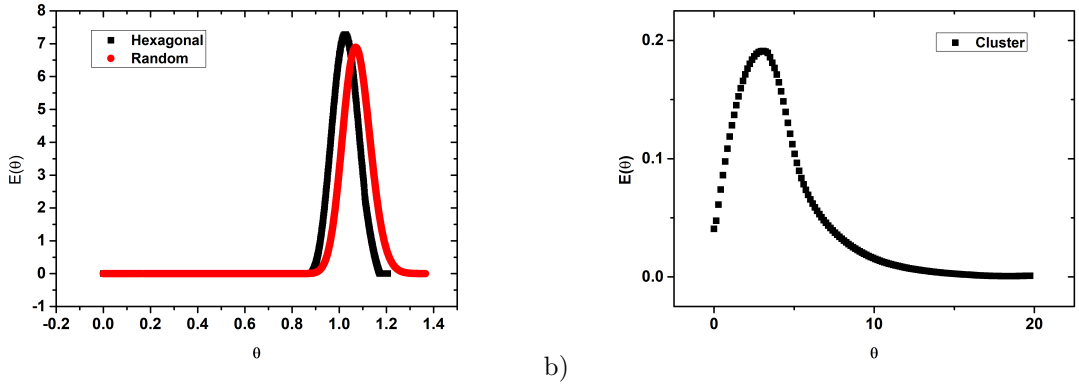


Fig. 7: Dimensionless time (t^*) of tracer concentration C for cluster arrangement of fibers.

transit times while random configurations induce moderate spreading. Finally, clustered microstructures generate pronounced dispersion with long-tailed RTDs and elevated mean residence times. The spatial arrangement of fibers, beyond volume fraction alone, is thus a key determinant of transient transport dynamics.

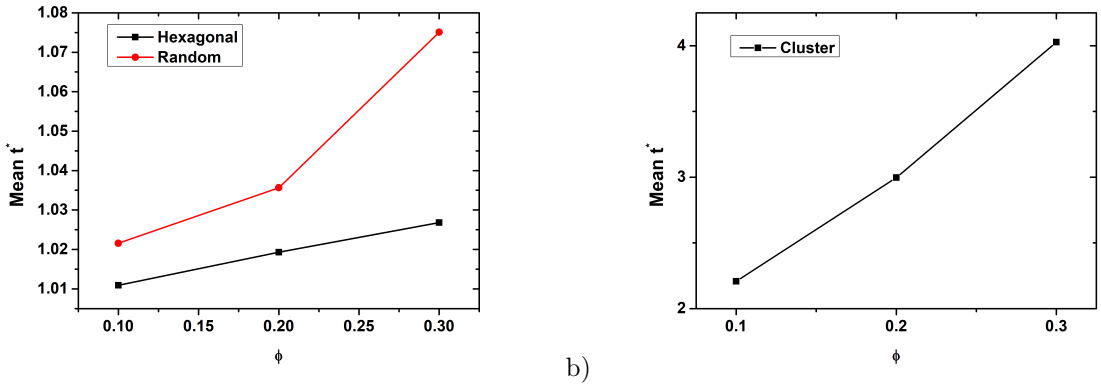
4 Discussion

The results presented in this study offer critical insights into how fiber arrangement, ϕ, and Pe affect the transport dynamics within fibrous media, particularly biological tissues. It should be emphasized that the present study is a fundamental investigation of



a) b)

Fig. 8: Normalized residence time distributions, E(θ), for different microstructural configurations at $Pe = 1$ and $\phi = 0.3$ for a) Ordered (hexagonal) and random fiber arrangements and b) Clustered configurations.

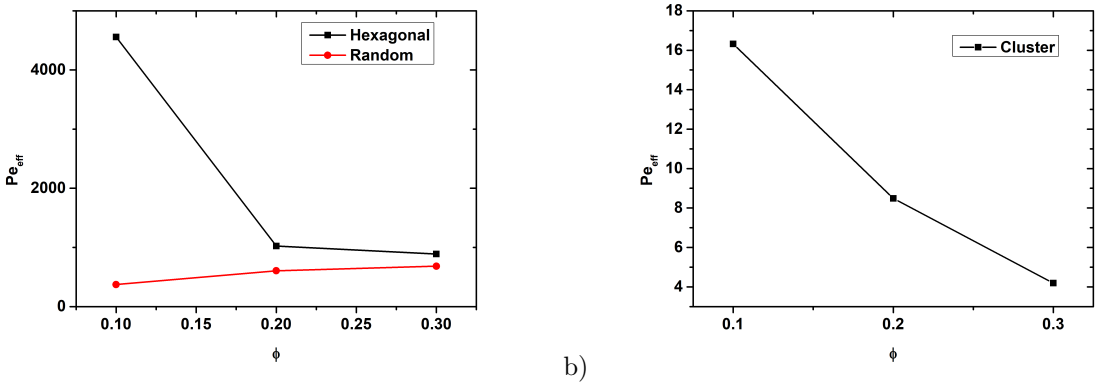


a) b)

Fig. 9: Mean dimensionless transit time, $\langle t^* \rangle$, as a function of fiber volume fraction ϕ at $Pe = 1$ for a) ordered (hexagonal), random and b) cluster arrangements.

microstructure-transport coupling in idealized two-dimensional fibrous porous media. The biological framing motivates the choice of geometry and parameter ranges, but it does not constitute a validated model of any specific tissue. Extrapolation to three-dimensional biological systems should therefore be treated as hypothesis-generating rather than predictive. Within this idealized framework, understanding these dynamics may still inform a range of applications, including fibrous scaffold design, drug delivery systems, and other engineered fibrous materials.

Figs 4 and 7 together illustrate how these three parameters shape breakthrough behavior across the ordered, random, and clustered microstructures. In low Pe, diffusion-dominated regimes, transport is slow and broadly distributed – a scenario



a) b)

Fig. 10: Effective Peclet number (Pe_{eff}) as a function of fiber volume fraction (ϕ) at $Pe = 1$ for a) the hexagonal, random and b) cluster microstrucures.

analogous to diffusion-limited nutrient delivery through dense ECM, as in cartilage. As Pe increases, breakthrough curves sharpen, resulting in faster, more predictable transport relevant to scaffolds exposed to dynamic flow (e.g. vascularized tissues), where optimizing porosity and fiber alignment can enhance convective delivery of nutrients and oxygen Langer and Peppas (2003). Fiber ϕ consistently modulates breakthrough time across all three arrangements, but its effect is markedly amplified by clustering. Unlike the weak (random) or negligible (hexagonal) ϕ-dependence of ordered and disordered arrays, clustered configurations show breakthrough times that scale strongly with ϕ (Fig. 7), reflecting the additional resistance imposed by dense fiber aggregates. These trends may carry qualitative implications for drug delivery design in fibrous media generally. This holds only if similar spatial organization persists in three-dimensional, physiologically representative geometries — a correspondence not established by the present two-dimensional study. Higher fiber density could, in principle, be exploited to prolong therapeutic release in such media, while lower density would favor more rapid delivery Shapiro and Cohen (1997). Translating these idealized trends to real tissue transport, however, requires further validation. The heterogeneous, disorganized ECM typical of tumor tissue is qualitatively reminiscent of the random and clustered geometries studied here Folkman (2002). However, the present two-dimensional fiber arrangements do not capture the three-dimensional connectivity, fiber waviness, or anisotropic remodeling characteristic of actual tumor ECM. Any inference about drug penetration in real tissue should therefore be treated as hypothesis-generating rather than predictive. Within this idealized picture, the broadened, irregular breakthrough curves associated with clustered arrangements are at least suggestive of the kind of transport heterogeneity that size-tunable nanoparticle carriers or ECM-modifying co-therapies are designed to address Maeda et al. (2000).

The moment-based analysis of the residence time distributions clarifies the physical origin of these differences. While porosity increases from $\phi = 0.1$ to 0.3 in all cases, the effective Pe does not follow a universal trend across microstructures: ordered

(hexagonal) configurations remain predominantly advective and narrowly distributed (high Pe_{eff}, limited variance), whereas clustered arrangements show a pronounced reduction in Pe_{eff} alongside substantial growth in residence-time variability.

The order-of-magnitude gap in Pe_{eff} between hexagonal and random arrangements at matched Pe and ϕ (Fig. 10a) is itself informative. The hexagonal lattice imposes identical, periodically repeating flow channels, so streamline path lengths stay uniform and cross-sectional velocity variance is low. The random arrangement, even before clustering, already produces a spread of channel widths and preferential "river" pathways (Fig. 3a). This introduces velocity variance, and hence dispersion, absent by construction in the ordered lattice.

This behavior cannot be attributed to solid fraction alone, and is consistent with spatial velocity heterogeneity induced by microstructural correlations, although a direct spatial correlation analysis was not performed here. Mechanistically, clustering introduces extended low-velocity regions and localized high-shear channels that increase the variance of the longitudinal velocity field. Since the longitudinal dispersion coefficient scales with velocity fluctuations and correlation length, consistent with classical dispersion theory for periodic porous media Edwards et al. (1993); Cussler (2009), the clustered topology enhances dispersive spreading even at identical nominal Pe. The resulting RTD broadening and long tails indicate multi-scale, correlation-dominated transport rather than purely porosity-controlled behavior. Dispersion here is governed by topology-induced velocity variance rather than by global geometric metrics alone.

These findings indicate that transport variability is fundamentally microstructure-driven rather than porosity-driven. Many biological tissues, such as tumor ECM, fibrotic regions, and remodeled vascularized scaffolds, exhibit heterogeneous, spatially correlated fiber arrangements rather than idealized ordered structures. The present results suggest that such clustering can substantially alter solute transit times, potentially leading to non-uniform drug exposure, delayed washout, and localized accumulation. This raises the possibility that scaffold topology could, in principle, be engineered to influence nutrient homogenization, oxygen penetration, and drug residence time. This offers a starting point for future predictive modeling of microstructural design in tissue engineering and drug delivery.

Several limitations should be noted. The flow field is represented in two dimensions. While this is appropriate for the Newtonian, transversally-uniform fiber geometries considered here, it does not capture three-dimensional effects such as fiber waviness, out-of-plane connectivity, or axial tortuosity variation present in real tissue microstructures. The molecular diffusion coefficient was held spatially uniform throughout, isolating the effect of velocity-field heterogeneity on RTD statistics but excluding the additional variability that spatially-varying apparent diffusivity would introduce in real tissue. While the flow solver was validated against an analytical permeability model, direct quantitative validation of the resulting RTD statistics against experimental or independently simulated fibrous-tissue transport data was beyond the scope of the present study. The $Pe_{eff} = 2/\sigma_\theta^2$, derived under a near-Gaussian RTD assumption, should be interpreted as a summary macrodispersion index rather than a literal Gaussian-equivalent Pe for the strongly right-skewed clustered $RTDs$ reported here.

Beyond the general dispersion-theory basis for periodic porous media Edwards et al. (1993), direct RTD data for fibrous or ECM-like biological transport systems are scarce in the literature, limiting quantitative benchmarking of the present results against comparable experimental or computational studies Kordas et al. (2018).

Finally, the mechanistic interpretation of clustering-induced macrodispersion offered above is not substantiated by a direct spatial correlation analysis. This remains, alongside experimental or three-dimensional validation, a direction for future work.

5 Conclusions

This study provides a comprehensive analysis of transport dynamics in biological tissues modeled as fibrous media, examining how fiber arrangement, ϕ, and Pe govern hydraulic permeability and residence time distributions. Beyond the qualitative breakthrough-curve trends, a moment-based RTD analysis, which evaluates the first and second statistical moments and the Pe_{eff}, provided a quantitative measure of microstructure-induced transport variability. This shows that dispersion is not governed solely by porosity but is strongly modulated by spatial organization.

The results establish a clear microstructural transport hierarchy, consistent across the investigated volume fractions. Ordered hexagonal configurations exhibited high Pe_{eff} and narrowly distributed transit times, consistent with quasi-plug-flow behavior and limited longitudinal dispersion. Random arrangements introduced moderate spreading, reflecting velocity-field heterogeneity from geometric disorder. Clustered microstructures produced pronounced right-skewed RTDs, elevated mean transit times, and a sharp reduction in Pe_{eff}, consistent with the emergence of localized low-velocity regions and correlation-driven macrodispersion. This mechanistic interpretation, however, was not directly verified through spatial correlation analysis. Collectively, this hierarchy shows that spatial organization, beyond porosity alone, is a primary regulator of transport efficiency in fibrous biological media. Within the two-dimensional, idealized framework adopted here, these results suggest a possible relevance to fibrous scaffold design and drug delivery. Specifically, controlling fiber arrangement and density, not porosity alone, could help govern transport predictability. Extension of this conclusion to real, three-dimensional tissue microstructures, however, remains to be established.

From a broader porous-media standpoint, these findings suggest that fiber topology could, in principle, be engineered to influence solute homogenization, penetration depth, and residence time in fibrous materials generally. Extending this reasoning to pathological tissues — where ECM remodeling and fiber clustering are common — is an appealing but currently unverified hypothesis. It would require three-dimensional, physiologically representative geometries and, ideally, comparison with experimental transport data before any claim of biological relevance can be made with confidence.

Overall, the present framework quantitatively links microstructural organization, residence time statistics, and effective transport parameters, offering a starting point for the design of fibrous biomaterials with tailored transport performance. The proposed methodology could, in principle, be extended to patient-specific or image-based

scaffold geometries and integrated into multiscale biomedical transport simulations, though such extensions remain untested.

Acknowledgments. The authors would like to acknowledge the support of the Greek Research & Technology Network (GRNET) for the computational time granted in the National HPC facility ARIS.

Declarations

Funding

This research did not receive any specific grant from funding agencies in the public, commercial, or not-for-profit sectors.

Competing Interests

The authors declare that they have no known competing financial interests or personal relationships that could have appeared to influence the work reported in this paper.

Ethics approval

Not applicable

Author Contributions

E.G.K. conceived and designed the study, performed the CFD and RTD simulations, and drafted the manuscript. A.T., P.C., and T.D.P. contributed to data analysis and interpretation and supervised the study. All authors reviewed and approved the final manuscript.

Data Availability

The datasets generated and/or analysed during the current study are available from the corresponding author on reasonable request.

References

Hu, M., Ling, Z., Ren, X.: Extracellular matrix dynamics: Tracking in biological systems and their implications. Journal of Biological Engineering **16**, 13 (2022)

Huang, J., Zhang, L., Wan, D., Zhou, L., Zheng, S., Lin, S., Qiao, Y.: Extracellular matrix and its therapeutic potential for cancer treatment. Signal Transduction and Targeted Therapy **6**, 153 (2021)

Bear, J.: Dynamics of Fluids in Porous Media. Dover Publications, Garden City, NY (1972)

Dullien, F.A.L.: Porous Media: Fluid Transport and Pore Structure. Academic Press, San Diego, CA (2012)

Kamm, R.D.: Cellular fluid mechanics. Annual Review of Fluid Mechanics **31**(1), 55–78 (1999)

Jain, R.K.: Transport of molecules across tumor vasculature. Cancer and Metastasis Reviews **6**(4), 559–593 (1987)

Sahimi, M.: Flow and Transport in Porous Media and Fractured Rock: From Classical Methods to Modern Approaches. Wiley-VCH, Weinheim, Germany (2011)

Dutta, D., Tarbell, J.M.: Influence of non-uniform wall shear stress on endothelial cell proliferation and apoptosis in a 3-D flow model. Annals of Biomedical Engineering **24**(4), 537–544 (1996)

Carmeliet, P., Jain, R.K.: Angiogenesis in cancer and other diseases. Nature **407**(6801), 249–257 (2000)

Murray, C.D.: The physiological principle of minimum work: I. the vascular system and the cost of blood volume. Proceedings of the National Academy of Sciences **12**(3), 207–214 (1926)

Jain, R.K.: Normalizing tumor vasculature with anti-angiogenic therapy: A new paradigm for combination therapy. Nature Medicine **11**(9), 987–989 (2005)

Griffith, L.G., Swartz, M.A.: Capturing complex 3D tissue physiology in vitro. Nature Reviews Molecular Cell Biology **7**(3), 211–224 (2006)

Saltzman, W.M.: Drug Delivery: Engineering Principles for Drug Therapy. Oxford University Press, New York, NY (2001)

Langer, R.: Drug delivery and targeting. Nature **392**(6679), 5–10 (1998)

Karvelas, E.G., Tsiantis, A., Papathanasiou, T.D.: Effect of micropolar fluid properties on the hydraulic permeability of fibrous biomaterials. Computer Methods and Programs in Biomedicine **185**, 105135 (2020)

Erisken, C., Tsiantis, A., Papathanasiou, T.D., Karvelas, E.G.: Collagen fibril diameter distribution affects permeability of ligament tissue: A computational study on healthy and injured tissues. Computer Methods and Programs in Biomedicine **196**, 105554 (2020)

Bhaskar, A., Singh, R.: Residence time distribution (RTD)-based control system for continuous pharmaceutical manufacturing process. Journal of Pharmaceutical Innovation **14**, 316–331 (2018)

Markicevic, B., Papathanasiou, T.D.: An explicit physics-based model for the transverse permeability of multi-material dual porosity fibrous media. Transport in Porous Media **53**, 265–280 (2003)

Markicevic, B., Papathanasiou, T.D.: A model for transverse permeability of bi-material layered fibrous preforms. Polymer Composites **24**(1), 68–82 (2004)

Burada, P.S., Hänggi, P., Marchesoni, F., Schmid, G., Talkner, P.: Diffusion in confined geometries. ChemPhysChem **10**, 45–54 (2009)

Hamada, M., Cueto-Felgueroso, L., Anna, P.: Diffusion limited mixing in confined media. Physical Review Fluids **5**(12), 124502 (2020)

Tsiantis, A., Papathanasiou, T.D.: A novel FastRSA algorithm: Statistical properties and evolution of microstructure. Physica A **534**, 122083 (2019)

Hassani, B., Hinton, E.: A review of homogenization and topology optimization II: Analytical and numerical solution of homogenization equations. Computers & Structures **69**(6), 719–738 (1998)

Hassani, B., Hinton, E.: Homogenization and Structural Topology Optimization. Springer, Berlin, Heidelberg (1999)

Feder, J.: Random sequential adsorption. Journal of Theoretical Biology **87**, 237–254 (1980)

Hinrichsen, E.L., Feder, J., Jossang, T.: Geometry of random sequential adsorption. Journal of Statistical Physics **44**, 793–827 (1986)

Geuzaine, C., Remacle, J.F.: Gmsh: a three-dimensional finite element mesh generator with built-in pre- and post-processing facilities. International Journal for Numerical Methods in Engineering **79**(11), 1309–1331 (2009)

Anderson, J.A., Glaser, J., Glotzer, S.C.: HOOMD-blue: A Python package for high-performance molecular dynamics and hard particle Monte Carlo simulations. Computational Materials Science **173**, 109363 (2020)

Weller, H.G., Tabor, G., Jasak, H., Fureby, C.: A tensorial approach to computational continuum mechanics using object-oriented techniques. Computers in Physics **12**, 620–631 (1998)

Papathanasiou, T.D.: A structure-oriented micromechanical model for viscous flow through square arrays of fibre clusters. Composites Science and Technology **56**, 1055–1069 (1996)

Papathanasiou, T.D., Lee, P.D.: Morphological effects on the transverse permeability of arrays of aligned fibers. Polymer Composites **18**, 197–208 (1997)

Gebart, B.: Permeability of unidirectional reinforcements for RTM. Journal of Composite Materials **26**, 1100–1133 (1992)

463 Langer, R., Peppas, N.A.: Advances in biomaterials, drug delivery, and bionanotech-
464 nology. AIChE Journal **49**(12), 2990–3006 (2003)

465 Shapiro, L., Cohen, S.: Novel alginate sponges for cell culture and transplantation.
466 Biomaterials **18**(8), 583–590 (1997)

467 Folkman, J.: Role of angiogenesis in tumor growth and metastasis. Seminars in
468 Oncology **29**(6), 15–18 (2002)

469 Maeda, H., Wu, J., Sawa, T., Matsumura, Y., Hori, K.: Tumor vascular permeability
470 and the EPR effect in macromolecular therapeutics: A review. Journal of Controlled
471 Release **65**(1–2), 271–284 (2000)

472 Edwards, D., Shapiro, M., Brenner, H.: Dispersion and reaction in two-dimensional
473 model porous media. Physics of Fluids A **5**, 837–848 (1993)

474 Cussler, E.L.: Diffusion: Mass Transfer in Fluid Systems. Cambridge University Press,
475 Cambridge, UK (2009)

476 Kordas, M., Pluskota, D., Rakoczy, R.: The characterization of the residence time
477 distribution in a fluid mixer by means of the information entropy. In: Ochowiak, M.,
478 Woziwodzki, S., Doligalski, M., Mitkowski, P. (eds.) Practical Aspects of Chemical
479 Engineering. Lecture Notes on Multidisciplinary Industrial Engineering. Springer,
480 Cham (2018)